COBEM 2021 26th International Congress of Mechanical Engineering
November 22-26, 2021, Virtual Congress, Brazil
ABCM Associação Brasileira de Engenharia e Ciências Mecânicas

COB-2021-1028
PHASE-FIELD MODEL FOR STRESS CORROSION CRACKING BASED ON CONTINUUM MECHANICS AND THE CONCEPT OF MICROFORCES

Murilo P. Rodrigues
muriloprudente@mecanica.coppe.ufrj.br
Suelen dos S. Sobrinho
ss.sobrinho@mecanica.coppe.ufrj.br
Fernando Duda
duda@mecanica.coope.ufrj.br
Programa de Engenharia Mecânica, COPPE, Universidade Federal do Rio de Janeiro
Cidade Universitária, Rio de Janeiro, CEP 21941-972, RJ, Brazil

Abstract. *This paper presents a continuum-mechanical derivation of a phase-field model for dissolution in elastic solids under stress. The solid is immersed in a binary solution containing the dissolved solid as one of its components. The solid-solution system is treated as a continuous enriched medium, where a smooth scalar field, the phase-field, is introduced to describe the solid-solution interface. Accordingly, the phase-field is chosen to vary between* 0 *(solid) and* 1 *(solution). The solid-solution interface is identified as a small region in which the phase-field variation between those values occurs. The primary variables of the theory are the solid displacement, solid concentration, and the phase field. The corresponding governing equations are obtained by combining the basic balances of the theory, namely the standard force balance, the solid content balance, and the microforce force balance, with a constitutive theory consistent with thermodynamics. To assess the predictive capability of the proposed approach, a particular version of it is single out for further investigation based on its numerical implementation on the open-source python library called FEniCS.*

Keywords: *Phase-Field Model, Stress Cracking, Continuum Mechanics*

1. INTRODUCTION

Corrosion is one of the most frequent forms of failure in the naval, chemical, construction, and mechanical industries. According to Koch *et al.* (2016), global economic loss in 2013 is estimated to be 2.5 trillion dollars annually, which corresponds to 3.4% of the global GDP (Gross Domestic Product). Furthermore, up to 35% of this cost could have been reduced by adopting control and prevention measures.

In general terms, McCafferty (2010) states that corrosion can be described as the degradation of materials due to chemical or electrochemical interactions with environments. In particular, Stress Corrosion Cracking (SCC) refers to a specific type of pitting corrosion due to the concurrent action of mechanical stress and corrosive environment (Nguyen *et al.* (2018)). One of the main challenges to be overcome by predictive models for SCC relies on describing the morphological complexity of the sharp evolving interface separating a solid component and its environment. Recently, this issue has been addressed by using phase-field models. See, for instance, Nguyen *et al.* (2018), Cui *et al.* (2021), and references cited therein.

In phase-field models, interfaces are treated as small regions across which a smooth scalar field, the phase field, undergoes large variations. And hence, the transition between phases is done smoothly. Phase-field models have been used with success in many areas. We can cite the work of Kobayashi (1993) and Ferreira *et al.* (2006) in solidification of materials, in lithium batteries dendritic growth studies as done by Hong and Viswanathan (2018), to predict brittle failure according to de Moraes *et al.* (2020) and even to generate data to be used in machine learning applications as presented by Goswami *et al.* (2020). Of particular relevance to SCC are the already mentioned works by Nguyen *et al.* (2018) and Cui *et al.* (2021).

The works mentioned above demonstrate the potentiality of phase-field models to describe SCC. Regardless of that, a systematic derivation of phase-field models for this kind of problem is still lacking. This paper presents a continuum-mechanical derivation of a phase-field model for material dissolution in elastic solid under stress. The derivation is based on the concept of microforces introduced by Gurtin and co-workers (see, for instance, Gurtin (1996)) and builds up the work initiated by Sobrinho (2019). We consider this work as the first step of an effort to describe consistent models for stress corrosion cracking.

2. THEORY

In this section, the fundamental equations that govern the SCC model based on the material dissolution will be derived. The mathematical formulation is defined using the principles of continuum mechanics and the concept of microforces. We begin by introducing the basic laws of the theory, namely the standard force balance, the microforce balance, the solid content balance, and the free energy imbalance. This step is followed by the development of a constitutive theory consistent with the free energy imbalance. Finally, by combining the basic balances with the constitutive theory, we arrive at the governing equations of the problem under consideration.

2.1 Basic laws

Throughout this paper, we consider the solid-solution system as a single body $\mathcal{B}$ and write all equations for arbitrary control volumes. The theory is based on the assumption that the solid undergoes small elastic deformations, where the displacement field is represented by $\nabla \mathbf{u}$, and the infinitesimal strain tensor is defined by:

$$\boldsymbol{E} = \frac{\nabla \mathbf{u} + \nabla \mathbf{u}^T}{2} \tag{1}$$

Further, we consider that the solution is stagnant, that is, solution flow is neglected. The solid fraction is denoted by c whereas phase field denoted by ϕ. It varies from $\phi = 1$ in the solution to $\phi = 0$ in the solution. See Figure 1.

2.1.1 Force balances

In this paper, we consider the phase field ϕ as an independent kinematical descriptor, and hence, following Gurtin (1996), we introduce an extra force system, henceforth called microforce system. The idea is to characterize, from the macroscopic viewpoint, the power expended by microstructural changes leading to the evolution of ϕ. That extra force system is described in terms of the following quantities: i) microstress vector $\boldsymbol{\xi}$; ii) body microforce density π, which in turn is the sum of two parts, one external (π_e) and the other internal (π_i). Further, the microforce system must be consistent with its own balance, the microforce balance:

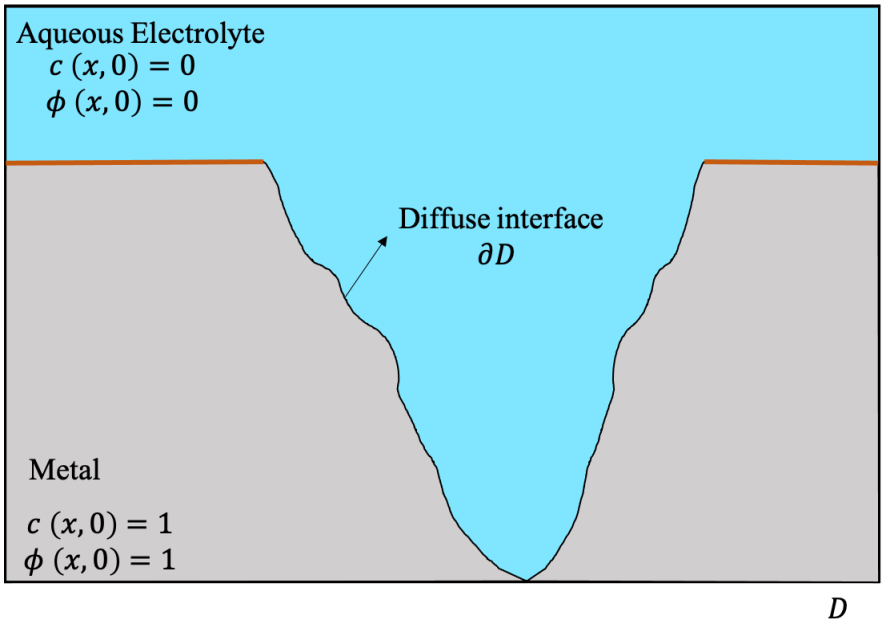

Figure 1. Schematic of the corrosion process in the phase field model.

The balance of microforces states that

$$\int_{\partial \mathcal{D}} \boldsymbol{\xi} \cdot \mathbf{n} \, dA + \int_{\mathcal{D}} \pi \, dV = 0 \tag{2}$$

for an arbitrary part $\mathcal{D}$ of $\mathcal{B}$ with outward unit normal field denoted by n. Applying the divergence and localization theorems, it follows from Eq. (2) that

$$div\boldsymbol{\xi} + \pi_i + \pi_e = 0 \tag{3}$$

must hold for arbitrary points in the interior of $\mathcal{B}$, where 'div' denotes the divergence operator.

As is well known, the standard force system by its turn is defined by stress tensor $\mathbf{S}$ and body force density $\mathbf{b}$ and the corresponding balance given by

$$\int_{\partial\mathcal{D}} \mathbf{Sn}\, dA + \int_{\mathcal{D}} \mathbf{b}\, dV = 0, \tag{4}$$

which localize into

$$div\mathbf{S} + \mathbf{b} = 0. \tag{5}$$

2.1.2 Solid content balance

Considering the diffusion of a single species (dissolved solid species) with density ρc, where c is the mass fraction and ρ is the density, for the control volume established in Fig. (1), the mass content is a control volume is defined as:

$$\int_{\mathcal{D}} \rho c\, dV \tag{6}$$

On defining $\mathbf{J}$ the ion mass flux from the dissolved material, the diffusion rate of ions in the material surface that is composed by the solid and liquid parts is given by:

$$\int_{\partial\mathcal{D}} \mathbf{J}\cdot\mathbf{n}\, dA \tag{7}$$

Deriving Eq. (6) to obtain the density rate and matching it with Eq. (7), we obtain the mass balance for the control volume as stated below.

$$\frac{\partial}{\partial t}\int_{\mathcal{D}} \rho c\, dV = -\int_{\partial\mathcal{D}} \mathbf{J}\cdot\mathbf{n}\, dA \tag{8}$$

After applying the divergence theorem, we rewrite Eq. (8) as

$$\frac{\partial}{\partial t}\int_{\mathcal{D}} \rho c\, dV + \int_{D} div\mathbf{J}\, dV = 0, \tag{9}$$

which, by recalling that $\mathcal{D}$ is time-independent, yields that

$$\int_{D} \rho\dot{c} dV + \int_{D} div\mathbf{J} dV = \int_{D} (\rho\dot{c} + div\mathbf{J}) dV = 0 \tag{10}$$

Applying the localization theorem in Eq. (10), we obtain the local form of the mass balance, which is given by:

$$\rho\dot{c} + div\mathbf{J} = 0 \tag{11}$$

2.1.3 Free energy imbalance

The subsequent step is to consider the mechanical version of the thermodynamics in the form of a free energy imbalance (Gurtin *et al.* (2009)):

$$\frac{\partial}{\partial t}\int_{\mathcal{D}} \rho\psi dV \leq T(\mathcal{D}) + W_0(\mathcal{D}) \tag{12}$$

where ψ is the free energy density,

$$T(\mathcal{D}) = -\int_{\partial\mathcal{D}} \mu\mathbf{J}\cdot\mathbf{n}\, dA \tag{13}$$

the energy inflow into $\mathcal{D}$ due to the ingress of ions, with μ representing the ion chemical potential, and

$$W_0(\mathcal{D}) = \int_{\partial\mathcal{D}} (\boldsymbol{\xi}\cdot\mathbf{n})\dot{\phi}\, dA + \int_{\mathcal{D}} \pi_e\cdot\dot{\phi}\, dV + \int_{\partial\mathcal{D}} \mathbf{S}\mathbf{n}\cdot\dot{\mathbf{u}}\, dA \tag{14}$$

the power expended on $\mathcal{D}$ by the macro and micro force balances. Using standard arguments, it can be shown that the above inequality localizes into

$$\rho\dot{\psi} - \boldsymbol{\xi}\cdot\nabla\dot{\phi} + \pi_i\dot{\phi} - \mathbf{S}\cdot\dot{\mathbf{E}} - \mathbf{J}\cdot\nabla\mu \leq 0 \tag{15}$$

2.2 Constitutive theory

Guided by Eq. (15), we consider that the list of independent and dependent constitutive variables to be given by $(c, \nabla\mu, \phi, \dot{\phi}, \nabla\phi, \mathbf{E})$ and $(\psi, \boldsymbol{\xi}, \pi_i, \mathbf{S}, \mu, \mathbf{J})$, respectively. Then, by invoking the Coleman-Noll procedure Coleman and Noll (1963), one can conclude that

- The free energy can depend on $(c, \phi, \nabla\phi, \mathbf{E})$ only, that is,

$$\psi = \hat{\psi}(c, \phi, \nabla\phi, \mathbf{E}), \tag{16}$$

  where $\hat{\psi}$ is the constitutive response for the free energy ψ;

- The constitutive responses $\hat{\mathbf{S}}$, $\hat{\mu}$, and $\hat{\boldsymbol{\xi}}$ for $\mathbf{S}$, μ, and $\boldsymbol{\xi}$ are determined by the constitutive response $\hat{\psi}$ by:

$$\begin{aligned}
\mathbf{S} &= \hat{\mathbf{S}}(c, \phi, \nabla\phi, \mathbf{E}) = \frac{\partial\hat{\psi}(c, \phi, \nabla\phi, \mathbf{E})}{\partial\mathbf{E}},\\
\mu &= \hat{\mu}(c, \phi, \nabla\phi, \mathbf{E}) = \frac{\partial\hat{\psi}(c, \phi, \nabla\phi, \mathbf{E})}{\partial c},\\
\xi &= \hat{\boldsymbol{\xi}}(c, \phi, \nabla\phi, \mathbf{E}) = \frac{\partial\hat{\psi}(c, \phi, \nabla\phi, \mathbf{E})}{\partial\nabla\phi};
\end{aligned} \tag{17}$$

- The constitutive responses $\hat{\pi}_i$ and $\hat{\mathbf{J}}$ for π_i and $\mathbf{J}$ must obey the *dissipation inequality*

$$\hat{\pi}_d(c, \nabla\mu, \phi, \dot{\phi}, \nabla\phi, \mathbf{E})\dot{\phi} + \hat{\mathbf{J}}(c, \nabla\mu, \phi, \dot{\phi}, \nabla\phi, \mathbf{E})\cdot\nabla\mu \leq 0 \tag{18}$$

  for all admissible $(c, \nabla\mu, \phi, \dot{\phi}, \nabla\phi, \mathbf{E})$, where

$$\hat{\pi}_d(c, \nabla\mu, \phi, \dot{\phi}, \nabla\phi, \mathbf{E}) := \hat{\pi}_i(c, \nabla\mu, \phi, \dot{\phi}, \nabla\phi, \mathbf{E}) - \frac{\partial\hat{\psi}(c, \phi, \nabla\phi, \mathbf{E})}{\partial\phi} \tag{19}$$

  is the dissipative part of the constitutive response $\hat{\pi}_i$.

2.3 A specialized theory and the corresponding governing equations

The preceding section has shows that the constitutive theory is fully specified by the constitutive responses $\hat{\psi}$, $\hat{\pi}_d$, and $\hat{\mathbf{J}}$. Following Sobrinho (2019), we henceforth assume that the free energy response is given by the sum of three parts, namely the gradient energy $\kappa|\nabla\phi|^2/2$, the chemical energy $f_c(c, \phi)$, and the elastic energy $f_e(\mathbf{E}, \phi)$. Therefore,

$$\hat{\psi}(c, \phi, \nabla\phi, \mathbf{E}) = \frac{\kappa}{2}|\nabla\phi|^2 + f_c(c, \phi) + f_e(\mathbf{E}, \phi), \tag{20}$$

where κ is a positive constant. As for $\hat{\pi}_d$ and $\hat{\mathbf{J}}$, we assume that

$$\hat{\pi}_d(c, \nabla\mu, \phi, \dot{\phi}, \nabla\phi, \mathbf{E}) = -\beta\dot{\phi} \quad \text{and} \quad \hat{\mathbf{J}}(c, \nabla\mu, \phi, \dot{\phi}, \nabla\phi, \mathbf{E}) = -M(1-\phi)\nabla\mu, \tag{21}$$

where β and M are positive parameters, which in turn assure that (18) is satisfied. The aforementioned choice for $\hat{\mathbf{J}}$ implies that ions are immobile in the solid phase ($\phi = 1$).

With the aforementioned choices, it follows that

$$\begin{aligned}
\hat{\mu} &= \frac{\partial f_c}{\partial c},\\
\hat{\boldsymbol{\xi}} &= \kappa\nabla\phi,\\
\hat{\pi}_i &= -\frac{\partial(f_c + f_e)}{\partial\phi} - \beta\dot{\phi},\\
\hat{\boldsymbol{S}} &= \frac{\partial f_e(\boldsymbol{E}, \phi)}{\partial\boldsymbol{E}},\\
\hat{\mathbf{J}} &= -M(1-\phi)\nabla\left(\frac{\partial f_c}{\partial c}\right)
\end{aligned} \quad . \tag{22}$$

Replacing Eq. $(22)_2$ and Eq. $(22)_3$ in microforce balance presented in Eq. (3) and rearranging it, is possible to obtain the Allen-Cahn equation, with the interface kinect parameter $\frac{1}{\beta}$

$$\dot{\phi} = \frac{1}{\beta}\left(-\frac{\partial f(c,\phi)}{\phi} + \alpha_\phi \nabla^2 \phi\right) \tag{23}$$

Similarly, replacing Eq. $(22)_1$ in Eq. (11) results in the diffusion equation

$$\dot{c} = div\left(M(1-\phi)\nabla\left(\frac{\partial f(c,\phi)}{\partial \phi}\right)\right). \tag{24}$$

The last step to develop the mathematical model that will represent the SCC problem is to determine the functions $f_c(c,\phi)$ and $f_e(\mathbf{E},\phi)$. For that, the Kim-Kim-Suzuki (KKS) model will be used to determine the function $f_c(c,\phi)$, the KKS model developed by Kim *et al.* (1999) assumes that the interface mixture has different compositions with the same chemical potential. That resumes to

$$c' = h(\phi)c_s + [1-h(\phi)]c_l \tag{25}$$

$$\frac{\partial f_s(c'_s)}{\partial c'_s} = \frac{\partial f_l(c'_l)}{\partial c'_l} \tag{26}$$

where $h(\phi)$ it the interpolation function that have the form $h(\phi) = -2\phi^3 + 3\phi^2$. In this function $h(\phi = 0) = 0$ and $(\phi = 1) = 1$, c'_s and c'_l are the normalized concentration in solid and liquid respectively. $f_s(c'_s)$ and $f_l(c'_l)$ are the free energy density in each phase. According to Kim *et al.* (1999), the free energy density is given by

$$f_c(c,\phi) = h(\phi)f_s(c'_s) + [1-h(\phi)]f_l(c'_l) + wg(\phi) \tag{27}$$

and $g(\phi)$ is the double well function usually represented by $g(\phi) = \phi^2(1-\phi)^2$.
The gradient energy (α_ϕ) and the potential height (w) are found using the relationship.

$$\sigma = \sqrt{16 w \alpha_\phi} \tag{28}$$

$$l = \alpha\sqrt{\frac{2\alpha_\phi}{w}} \tag{29}$$

where α is a constant equal to 2.94 and is used to define the interface in the range of $0,05 < \phi < 0,95$, σ is the surface tension and l is the interface thickness.

The elastic free energy density $f_e(\mathbf{E},\phi)$ is defined following Duda *et al.* (2018), which defines it as

$$f(\boldsymbol{E},\phi) = \phi^2\left[\frac{\lambda}{2}(tr\boldsymbol{E})^2 + G|\boldsymbol{E}|^2\right], \tag{30}$$

Where λ and G are the Lamé parameters. Notice that the elastic energy vanishes in the solution phase ($\phi = 0$).

3. NUMERICAL IMPLEMENTATION

Using the FEniCS framework for solving Partial Derivative Equations (PDEs), the first problem was studied to verify the model behavior. The first problem can be configured as a calibration problem since the parameters will be adjusted to approximate the phase-field model with the analytical solution.

The chosen problem was the pencil electrode test, which consists of a metal wire with $150\mu m$ in height, with the sides insulated by a coat of epoxy in order to leave only the top surface is exposed to the environment, as shown in Fig (2). The corrosion was considered symmetric within the electrode diameter, thus leading to a one-dimensional approximation for the model.

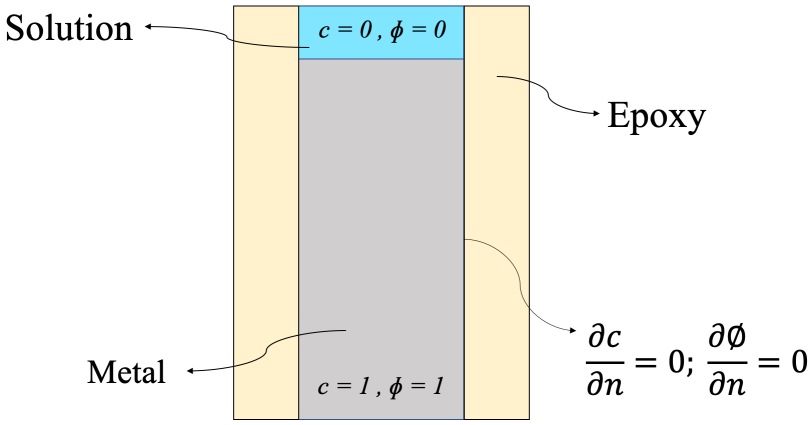

Figure 2. Pencil electrode test schematic, with Dirichlet boundary conditions on top and bottom surfaces and Neumann boundary condition on the sides.

In this test problem, Dirichlet boundary conditions are used for the solution and the metal, respectively $c = 0, \phi = 0$ and $c = 1, \phi = 1$. The sides of the metal wire are assigned a Neumann boundary condition which states that $\frac{\partial c}{\partial n} = 0$ and $\frac{\partial \phi}{\partial n} = 0$

In this problem, the analytical solution as defined per Scheiner and Hellmich (2007) states that the equation that governs the pit surface is:

$$x_d = 2\xi_d\sqrt{Dt} \tag{31}$$

being the unknown ξ_d defined by:

$$\frac{c_{sat}}{c_{solid} - c_{sat}} exp(-\xi_d^2) = \sqrt{\pi}\xi_d erf(\xi_d) \tag{32}$$

With the analytical solution, it is possible to verify that the pit depth is proportional to $\sqrt{t}$ and the corrosion is assumed to be diffusion-controlled.

In the phase-field model the transition from solid and liquid is calibrated with the parameter $L = \frac{1}{\beta}$. The higher the value of L, the higher the transition between phases controlled per activation and diffusion. It is important to highlight that it is not necessary to indicate a boundary condition on the interface.

The weak formulation is obtained by multiplying Eq. (23) and Eq. (24) for a test function each and integrating second-order derivatives per part. It is essential to clarify that the external forces acting on the body are being disregarded for this first model. That is why Eq. $(22)_4$ is not represented in this simulation.

$$\int \dot{\phi} v \, dx = -L \int 2A(c + c_{le}[h(\phi) - 1] - h(\phi))h'(\phi)(c_{le} - 1)v \, dx - Lw \int g'(\phi)v \, dx - L\alpha_\phi \int \frac{d\phi}{dx}\frac{dv}{dx} \, dx \tag{33}$$

$$\int \dot{c} q \, dx = -D \int \frac{dc}{dx}\frac{dq}{dx} + 2D(c_{le} - 1) \int \frac{d\phi^3}{dx}\frac{dq}{dx} - 3D(c_{le} - 1) \int \frac{d\phi^2}{dx}\frac{dq}{dx} \tag{34}$$

Where v and q are the test functions.

4. PRELIMINARY RESULTS

The results obtained for this first model show that the model's behavior is similar to what is expected from the numerical solution, albeit the results are not the same as the analytical model.

Figure (3) shows the evolution of c', and ϕ on the interface between solid and liquid. The red line represents the order parameter, and the dashed black line represents c'. It is possible to observe that c' evolves until it reaches the saturation concentration, represented by the blue dot.

Figure (4) shows the evolution of the model while the parameter L is increased, it is possible to identify that albeit the model is not reaching the analytical solution, increasing the value of L may lead to a solution that is consistent with the analytical model.

If high values of L are used, corrosion is expected to be higher than the analytical solution. This means that corrosion depth is excepted to be higher than the correct solution.

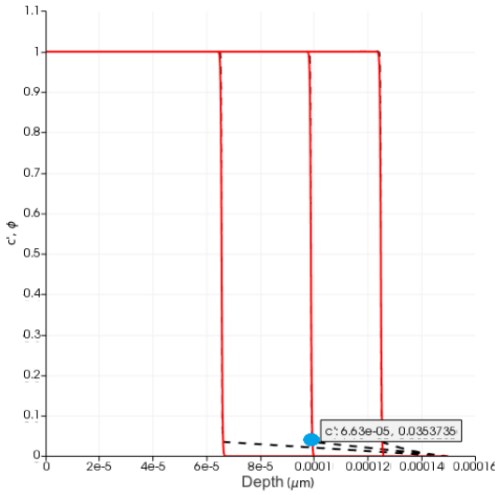

Figure 3. c' and ϕ evolution in the interface. Source: Adapted from Sobrinho (2019)

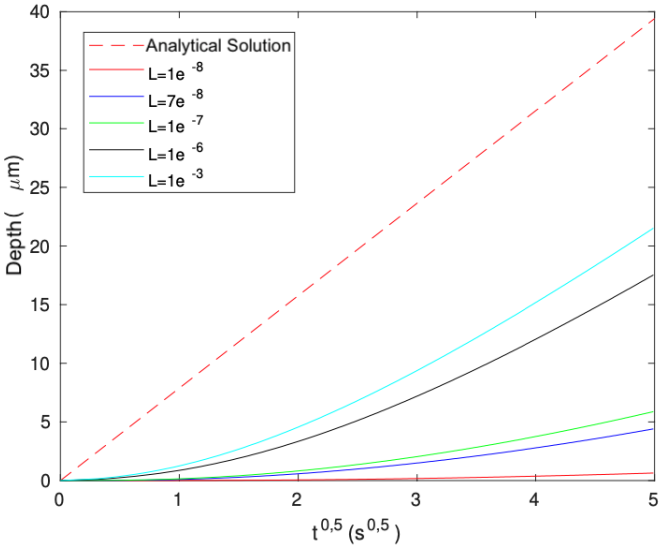

Figure 4. Analytical and simulation solution's comparison. Source: Adapted from Sobrinho (2019)

5. CONCLUDING REMARKS

A continuum-mechanical derivation of phase-field models for the dissolution of elastic solids under stress was presented in this paper. We discussed a simple one-dimensional example in which stress effects were neglected. Regardless of its simplicity, the preliminary results were promising to calibrate the model to match the analytical solution. With the calibration completed, it is possible to include the mechanical effects in the model and compare it with other classic simulations to validate the proposed phase-field model. The treatment advanced in this paper can be considered the first step towards formulating consistent phase-field models for stress corrosion cracking.

6. REFERENCES

Coleman, B.D. and Noll, W., 1963. "The thermodynamics of elastic materials with heat conduction and viscosity". *Archive for Rational Mechanics adn Analysis*, Vol. 13, pp. 167–178. doi:https://doi-org.ez29.periodicos.capes.gov.br/10.1007/BF01262690.

Cui, C., Ma, R. and Martínez-Pañeda, E., 2021. "A phase field formulation for dissolution-driven stress corrosion cracking". *Journal of the Mechanics and Physics of Solids*, Vol. 147, p. 104254. ISSN 0022-5096. doi:https://doi.org/10.1016/j.jmps.2020.104254. URL `https://www.sciencedirect.com/science/article/pii/S0022509620304622`.

de Moraes, E.A.B., Salehi, H. and Zayernouri, M., 2020. "Data-driven failure prediction in brittle materials: A phase-field

based machine learning framework".

Duda, F., Ciarbonetti, A., Toro, S. and Huespe, A., 2018. "A phase-field model for solute-assisted brittle fracture in elastic-plastic solids". *International Journal of Plasticity*, Vol. 102, pp. 16–40. ISSN 0749-6419. doi:https://doi.org/10.1016/j.ijplas.2017.11.004. URL https://www.sciencedirect.com/science/article/pii/S0749641917304552.

Ferreira, A.F., da Silva, A.J. and de Castro, J.A., 2006. "Simulation of the solidification of pure nickel via the phase-field method". *Materials Research*, Vol. 9, pp. 349–356.

Goswami, S., Anitescu, C., Chakraborty, S. and Rabczuk, T., 2020. "Transfer learning enhanced physics informed neural network for phase-field modeling of fracture". *Theoretical and Applied Fracture Mechanics*, Vol. 106, p. 102447. ISSN 0167-8442. doi:https://doi.org/10.1016/j.tafmec.2019.102447. URL https://www.sciencedirect.com/science/article/pii/S016784421930357X.

Gurtin, M.E., 1996. "Generalized ginzburg-landau and cahn-hilliard equations based on a microforce balance". *Physica D: Nonlinear Phenomena*, Vol. 92, No. 3, pp. 178–192. ISSN 0167-2789. doi:https://doi.org/10.1016/0167-2789(95)00173-5. URL https://www.sciencedirect.com/science/article/pii/0167278995001735.

Gurtin, M.E., Fried, E. and Anand, L., 2009. *The Mechanics and Thermodynamics of Continua*. Cambridge University Press, Cambridge.

Hong, Z. and Viswanathan, V., 2018. "Phase-field simulations of lithium dendrite growth with open-source software". *ACS Energy Letters*, Vol. 3, pp. 1737–1743.

Kim, S.G., Kim, W.T. and Suzuki, T., 1999. "Phase-field model for binary alloys". *Phys. Rev. E*, Vol. 60, pp. 7186–7197. doi:10.1103/PhysRevE.60.7186. URL https://link.aps.org/doi/10.1103/PhysRevE.60.7186.

Kobayashi, R., 1993. "Modeling and numerical simulations of dendritic crystal growth". *Physica D*, Vol. 63, pp. 410–423.

Koch, G., Varney, J., Thompson, N., Moghissi, O., Gould, M. and Payer, J., 2016. *Internation Measures of Prevention, Application and Economics of Corrosion Technologies Study*. Nace International, Houston, TX. URL http://impact.nace.org/documents/Nace-International-Report.pdf.

McCafferty, E., 2010. *Introduction to Corrosion Science*. Springer Science and Business Media, New York.

Nguyen, T.T., Bolivar, J., Shi, Y., Réthoré, J., King, A., Fregonese, M., Adrien, J., Buffiere, J.Y. and Baietto, M.C., 2018. "A phase field method for modeling anodic dissolution induced stress corrosion crack propagation". *Corrosion Science*, Vol. 132, pp. 146–160. ISSN 0010-938X. doi:https://doi.org/10.1016/j.corsci.2017.12.027. URL https://www.sciencedirect.com/science/article/pii/S0010938X17305875.

Scheiner, S. and Hellmich, C., 2007. "Stable pitting corrosion of stainless steel as diffusion-controlled dissolution process with a sharp moving electrode boundary". *Corrosion Science*, Vol. 49, No. 2, pp. 319–346. ISSN 0010-938X. doi:https://doi.org/10.1016/j.corsci.2006.03.019. URL https://www.sciencedirect.com/science/article/pii/S0010938X0600165X.

Sobrinho, S.d.S., 2019. *Modelo Continuo para Dissolução em Sólidos Elásticos Sob Tensão*. Master's thesis, Universidade Federal do Rio de Janeiro. URL https://w1files.solucaoatrio.net.br/atrio/ufrj-pem$_u pl//THESIS/1945/pemufrj2019mscsuelendossantossobrinho_20190517110300696.pdf$.

7. RESPONSIBILITY NOTICE

The authors are solely responsible for the printed material included in this paper.